Supplementary Information (SI) for Nanoscale.

Grazing-incidence x-ray diffraction elucidates structural correlations in fluid lipid and surfactant monolayers

– Supporting Information –

Joshua Reed,[†] Miriam Grava,[†] Gerald Brezesinski,[†] Chen Shen,[‡] and Emanuel Schneck*,[†]

†*Institute for Condensed Matter Physics, Technische Universität Darmstadt, Hochschulstrasse 8, 64289 Darmstadt, Germany*

‡*Deutsches Elektronen-Synchrotron DESY, Notkestrasse 85, 22607 Hamburg, Germany*

E-mail: emanuel.schneck@pkm.tu-darmstadt.de

Electron density layer model parameters as determined by GIXOS

Table S1: Parameters of the HC and HG layer in the electron density profiles as obtained by GIXOS. [a]Fixed according to our earlier work (refs. [1,2]). [b]In good agreement with the value reported earlier for a different surfactant (ref. [3]).

	DMPC				POPC			C_{12}DMPO
param. / Π (mN/m)	10	20	30	35	10	20	30	43
$\sigma_{air/HC}$ [Å] (±0.5)	2.5	2.6	2.6	2.7	2.7	2.7	2.7	2.0
d_{HC} [Å] (±0.5)	9.2	10.7	11.6	12.1	10.7	12.0	13.0	6.3
ρ_{HC} [e^-/Å^3]	0.30[a]	0.30[a]	0.30[a]	0.30[a]	0.30[a]	0.30[a]	0.30[a]	0.26[b]
$\sigma_{HC/HG}$ [Å] (±0.5)	3.6	2.2	2.2	2.2	2.7	2.2	2.3	2.3
d_{HG} [Å] (±0.5)	7.6	8.0	8.0	8.3	7.1	7.8	8.0	8.5
ρ_{HG} [e^-/Å^3] (±0.02)	0.43	0.43	0.44	0.45	0.39	0.41	0.45	0.35
$\sigma_{HG/wat}$ [Å](±0.5)	1.8	1.7	1.8	1.8	1.6	1.5	2.1	2.3

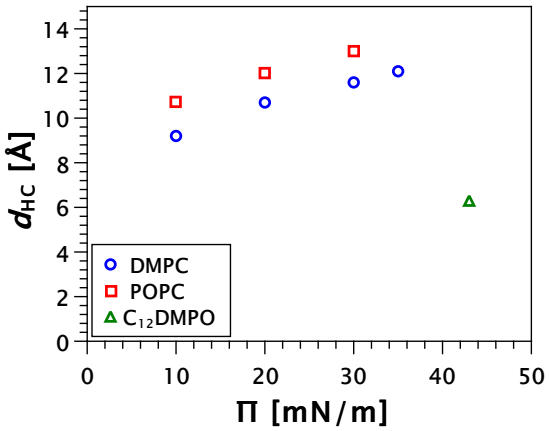

Figure S1: Hydrocarbon chain layer thickness d_{HC} of DMPC, POPC, and C_{12}DMPO monolayers as obtained by GIXOS as a function of the lateral pressure Π.

Total measured peak intensity

We define the measured total peak intensity $I_{\mathrm{tot}}^{\mathrm{m}}$ as the product of the peak height and the peak widths in Q_{xy} and Q_z directions, $I_{\mathrm{tot}}^{\mathrm{m}} = I_{\max} w_{xy} w_z$. In Fig. S2, $I_{\mathrm{tot}}^{\mathrm{m}}$ is plotted as a function of $f_{\mathrm{c}}/A_{\mathrm{mol}}^{\mathrm{a}}$. The linear relation between $I_{\mathrm{tot}}^{\mathrm{m}}$ and $f_{\mathrm{c}}/A_{\mathrm{mol}}^{\mathrm{a}}$ is indicated with a linear fit through the origin.

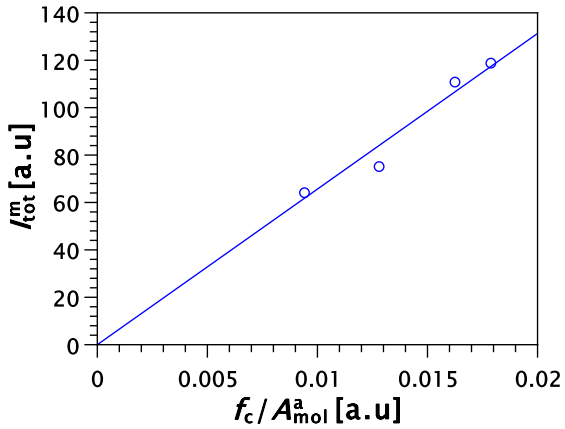

Figure S2: Representative comparison of the measured and predicted peak intensities for DMPC. The straight solid line through the origin is a linear fit of the data points.

Compression moduli $K_{\mathbf{A}}^{\mathbf{c}}$ and $K_{\mathbf{A}}$ of ordered monolayers

Octadecanol is a prime example to discuss the lateral compressibility of highly ordered monolayers. The phase behavior of octadecanol monolayers at the air/water interface has been studied by standard isotherm experiments, Brewster-angle microscopy (BAM), and GIXD.[4–8] At low Π, the molecules are tilted in the next-nearest neighbor direction (both diffraction peaks are located at $Q_z \neq 0$). Above the tilting transition, the S phase, characterized by non-tilted molecules arranged in a centered rectangular (distorted hexagonal) lattice (two diffraction peaks at $Q_z = 0$), is formed at low temperatures. At higher temperatures, only one first-order diffraction peak (LS phase) can be seen in the powder pattern. The LS phase is optically isotropic.[9] Although there is no direct evidence of hexatic order, there are several indirect arguments in favor of such attribution.[10] The lateral compressibility of octadecanol monolayers has been determined in the isotropic LS phase[8] from measurements of $A_{\mathrm{mol}}^{\mathrm{c}}(\Pi)$, where the compression modulus $K_{\mathrm{A}}^{\mathrm{c}}(\Pi)$ can also be expressed according to Eq. 7 in the main text. The data can be compared with $K_{\mathrm{A}}(\Pi)$ reconstructed from the isotherm $\Pi(A_{\mathrm{mol}}^{\mathrm{a}})$ provided in reference.[4] Both data sets were obtained at T = 20 °C. Fig. S3 A compares $\Pi(A_{\mathrm{mol}}^{\mathrm{c}})$ and $\Pi(A_{\mathrm{mol}}^{\mathrm{a}})$, where always $A_{\mathrm{mol}}^{\mathrm{c}} \leq A_{\mathrm{mol}}^{\mathrm{a}}$ at the same pressure, as expected. The ordered fraction, f_{o}, has been calculated by using Eq. 6 (main text) and is presented in Fig. S3 B as a function of Π. The ordered fraction increases almost linearly with Π. Interestingly, f_{o} is at all pressures very close to 1. This shows, that the defects make up not more than 3-4% of the total monolayer area even at the lowest pressure. For monolayers undergoing the direct transition from the gaseous phase to a condensed phase (re-sublimation), the condensed islands are already formed during spreading. The defects will therefore depend on the solvent and the spreading conditions. No annealing procedure has been applied in both studies.[4,8]

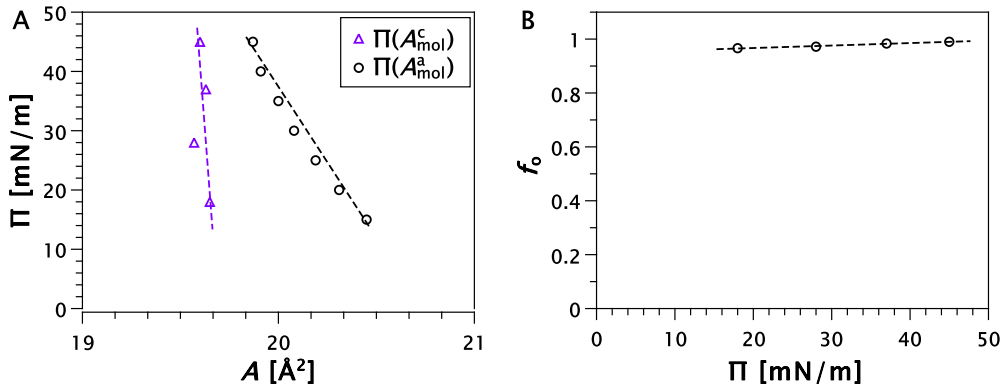

Figure S3: (A) $\Pi(A^{\mathrm{a}}_{\mathrm{mol}})$ and $\Pi(A^{\mathrm{c}}_{\mathrm{mol}})$ for octadecanol monolayers at T = 20 °C in the isotropic LS phase. Dashed lines are linear fits from which K_{A} and $K^{\mathrm{c}}_{\mathrm{A}}$ are deduced. (B) The ordered fraction f_{o} as a function of the lateral pressure Π.

The compression moduli $K^{\mathrm{c}}_{\mathrm{A}}(\Pi)$ and $K_{\mathrm{A}}(\Pi)$ are compared in Fig. S4. In contrast to the LE phase, in which the compression modulus $K^{\mathrm{c}}_{\mathrm{A}}$ decreases gradually with increasing pressure, $K^{\mathrm{c}}_{\mathrm{A}}$ virtually does not change with compression (variations in Π), indicating that the packing density of the octadecanol molecules in the isotropic LS phase is not influenced by compression. Looking at the numbers at high Π, $K^{\mathrm{c}}_{\mathrm{A}}$ is roughly 150 times larger in the LS phase compared to the LE phase. K_{A} decreases only marginally upon compression in the LS phase. Remarkably, K_{A} is significantly smaller (factor of 15) than $K^{\mathrm{c}}_{\mathrm{A}}$. Even if the defects make up only few % of the total area, they obviously have a large influence on K_{A}.

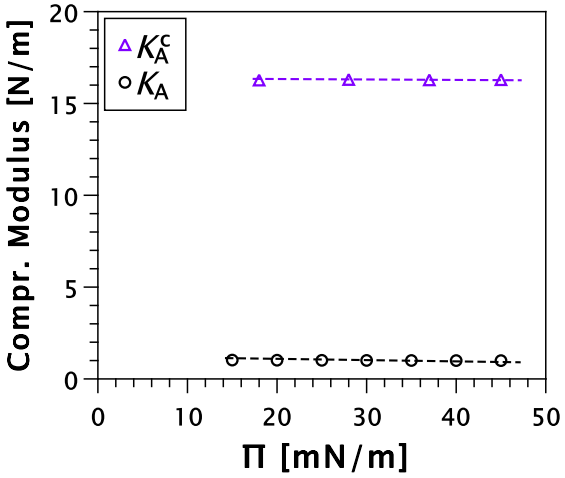

Figure S4: Compression moduli K_{A} and $K^{\mathrm{c}}_{\mathrm{A}}$ of an octadecanol monolayer at 20 °C in the isotropic LS phase.

Average number of phospholipids in a structurally correlated region

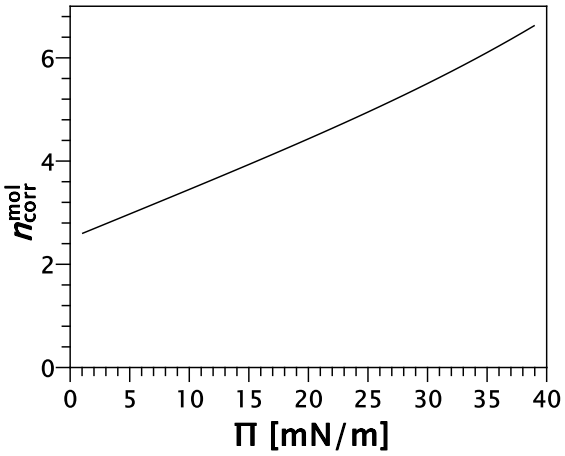

Figure S5: Average number of phospholipids in a structurally correlated region, $n_{\mathrm{mol}}^{\mathrm{corr}}$, as a function of the lateral pressure Π. The curve is derived from Eqs. 3 - 5 and from the linear fit in Fig. 6 D (all in the main text), as $n_{\mathrm{mol}}^{\mathrm{corr}}(\Pi) = A_{\mathrm{corr}}(\Pi)/A_{\mathrm{mol}}^{\mathrm{c}}(\Pi)$.

Determination of $A_{\mathrm{mol}}^{\mathrm{a}}$ of C_{12}DMPO at Π = 43 mN/m with total-reflection x-ray fluorescence (TRXF)

$A_{\mathrm{mol}}^{\mathrm{a}} \approx 35.5$ Å^2 was obtained according to Eq. (5) in ref.[11] from our measurements at the beamline P08 of storage ring PetraIII with a setup described in ref.[2] The reference system for the P fluorescence intensity calibration was a Langmuir monolayer of 1,2-distearoyl-*sn*-glycero-3-phosphocholine (DSPC) at Π = 30 mN/m, and for exclusion layer thickness for C_{12}DMPO we assumed $d = d_{\mathrm{HC}}$ = 0.6 nm (see Table S1 and ref.[12] for further details).

Meta-stability of lipid monolayers in the LC phase

The equilibrium spreading pressure (Π_{eq}) is an experimental value based on the true thermodynamic equilibrium (in terms of equal chemical potential) between a monolayer and its solid bulk

form at the air/liquid interface. The conditions at which spreading occurs depend on the particular crystal structure of the amphiphile. Phosphatidylcholine lipids are exceptional as they only commence spreading as chain-melting occurs. With water-insoluble fatty acids and alcohols it has been well established[13] that $d\Pi_{eq}/dT$ changes sign when chain melting occurs. The maximum equilibrium spreading pressure of monolayers of fatty acid esters coincides with the melting temperatures.[14] The determination of Π_{eq} is important because it signifies the pressure at which spread monolayers become thermodynamically unstable with respect to the corresponding bulk lipid phase. Compressing the monolayer to surface pressures above Π_{eq} leads to the monolayer collapse and the formation of the surfactant bulk phase.[15] However, the kinetics of this collapse can be extremely slow so that monolayers can be over-compressed to form meta-stable films. When the bulk phase is liquid-like, collapse usually occurs at Π_{eq} and the monolayers cannot be significantly over-compressed. In contrast, when the bulk lipid is crystalline, an activation energy to collapse first has to be overcome, which often allows for a considerable over-compression of the monolayer. This is why monolayers of phosphatidylcholine lipids in the LC phase can be typically compressed to very high lateral pressures.[16,17]

References

(1) Grava, M.; Ibrahim, M.; Sudarsan, A.; Pusterla, J.; Philipp, J.; Rädler, J. O.; Schwierz, N.; Schneck, E. Combining molecular dynamics simulations and x-ray scattering techniques for the accurate treatment of protonation degree and packing of ionizable lipids in monolayers. The Journal of Chemical Physics **2023**, 159, 154706.

(2) Mortara, L.; Mukhina, T.; Chaimovich, H.; Brezesinski, G.; van der Vegt, N. F.; Schneck, E. Anion Competition at Positively Charged Surfactant Monolayers. Langmuir **2024**,

(3) Kanduč, M.; Schneck, E.; Stubenrauch, C. Intersurfactant H-bonds between head groups of n-dodecyl-β-d-maltoside at the air-water interface. Journal of colloid and interface science **2021**, 586, 588–595.

(4) Lawrie, G.; Barnes, G. Octadecanol monolayers: the phase diagram. Journal of colloid and interface science **1994**, 162, 36–44.

(5) Lautz, C.; Fischer, T. M. Discontinuities in the Tilt Angle of Octadecanol Langmuir Monolayers As Observed with Brewster Angle Autocorrelation Spectroscopy. The Journal of Physical Chemistry B **1997**, 101, 8790–8793.

(6) Brezesinski, G.; Kaganer, V.; Möhwald, H.; Howes, P. Structure of octadecanol monolayers: An x-ray diffraction study. The Journal of chemical physics **1998**, 109, 2006–2010.

(7) Kaganer, V.; Brezesinski, G.; Möhwald, H.; Howes, P.; Kjaer, K. Positional order in Langmuir monolayers. Physical review letters **1998**, 81, 5864.

(8) Kaganer, V.; Brezesinski, G.; Möhwald, H.; Howes, P.; Kjaer, K. Positional order in Langmuir monolayers: An x-ray diffraction study. Physical Review E **1999**, 59, 2141.

(9) Riviere, S.; Hénon, S.; Meunier, J.; Schwartz, D. K.; Tsao, M.-W.; Knobler, C. M. Textures and phase transitions in Langmuir monolayers of fatty acids. A comparative Brewster angle microscope and polarized fluorescence microscope study. The Journal of chemical physics **1994**, 101, 10045–10051.

(10) Kaganer, V. M.; Möhwald, H.; Dutta, P. Structure and phase transitions in Langmuir monolayers. Reviews of Modern Physics **1999**, 71, 779.

(11) Mukhina, T.; Pabst, G.; Ruysschaert, J.-M.; Brezesinski, G.; Schneck, E. pH-Dependent physicochemical properties of ornithine lipid in mono-and bilayers. Physical Chemistry Chemical Physics **2022**, 24, 22778–22791.

(12) Brezesinski, G.; Schneck, E. Investigating ions at amphiphilic monolayers with X-ray fluorescence. Langmuir **2019**, 35, 8531–8542.

(13) Gaines Jr, G. L. Insoluble monolayers at liquid-gas interfaces. Wiley-Interscience, New York **1966**,

(14) Rettig, W.; Kuschel, F. A first-order transition between the liquid-expanded and the liquid-condensed phases in insoluble monolayers of fatty acid esters as detected by measurement of equilibrium spreading pressure. Journal of colloid and interface science **1990**, 140, 169–174.

(15) Phillips, M.; Hauser, H. Spreading of solid glycerides and phospholipids at the air—water interface. Journal of Colloid and Interface Science **1974**, 49, 31–39.

(16) Joos, P.; Demel, R. The interaction energies of cholesterol and lecithin in spread mixed monolayers at the air-water interface. Biochimica et Biophysica Acta (BBA)-Biomembranes **1969**, 183, 447–457.

(17) Watkins, J. The surface properties of pure phospholipids in relation to those of lung extracts. Biochimica et Biophysica Acta (BBA)-Lipids and Lipid Metabolism **1968**, 152, 293–306.